JOURNAL OF AIRCRAFT
Vol. 39, No. 6, November–December 2002

Investigation on Transonic Convex-Corner Flows

Kung-Ming Chung*
National Cheng Kung University, Tainan 711, Taiwan, Republic of China

An experimental investigation was conducted to study the transonic flow past convex corners. The mean surface pressure indicated strong inviscid–viscous interactions, and the interaction region increased with the freestream Mach number and the convex-corner angle. Unsteadiness of the interaction was characterized by an intermittent region and a local peak pressure fluctuation. The peak pressure fluctuations and the tentative boundary between the attached and separated flows could be scaled with the convex-corner angle and a second-order freestream Mach number ($M_\infty^2 \eta$).

Nomenclature

C_p = pressure coefficient, $(p_w - p_\infty)/q_\infty$
C_{σ_p} = pressure fluctuation coefficient, $(\sigma_p - \sigma_{p,\infty})/q_\infty$
M_∞ = Mach number
p = pressure
q_∞ = dynamic pressure
Re = Reynolds number
U_∞ = freestream velocity
x = coordinate along the surface of the corner
x^* = x/δ_0
δ_0 = incoming boundary-layer thickness
η = convex-corner angle, positive downward, deg
σ_p = rms pressure fluctuation

Introduction

FLOW around a transonic airfoil or deflected control surface is critical to the aerodynamic characteristics and performance of an aircraft. The typical feature on a transonic airfoil is associated with a quasi-normal shock on the upper surface. When the shock is strong enough, development of separation bubble changes the flowfield significantly and increases the drag.[1,2] A study by Liu and Squire[3] indicated that separation of a circular-arc model can be classified as trailing-edge separation or shock-induced separation. For the type of trailing-edge separation, the boundary layer separates around the trailing edge due to the adverse pressure gradient when the peak Mach number upstream of shock position is relatively small. At the critical peak Mach number, the shock wave is strong enough to separate the boundary layer just under the shock foot. This is known as the shock-induced separation. In the Liu and Squire's study, the critical peak Mach number $M_{p,\mathrm{cr}}$ is about 1.3, and it appears to be independent of the boundary-layer thickness-to-radius (δ/R) ratio of the curve surface. The maximum length of separation is observed at $M_{p,\mathrm{cr}}$ for all values of δ/R.

In addition, aircraft performance improvement is always one of the major goals. Bolonki and Gilyard indicated[4] that deflected control surfaces could be used in combination to provide variable camber control within the operational flight envelopes. The active modification of the control surfaces could potentially play a role in performance optimization for an aircraft, and benefits of variable camber using a simple trailing-edge control surface system can approach more than 10%. At the transonic speeds, it is known that increasing camber at the trailing edge can result in maximizing lift-to-drag ratio and a higher buffet boundary.[5] However, the critical Mach number, onset of boundary-layer separation, and drag are also strongly related to the allowable deflection of the control surfaces. In particular, the boundary layer near the trailing edge of a conventional highly loaded transonic airfoil is considerably weakened due to the steep pressure gradient. Small deflection of the control surfaces may evoke separation.[6] A great deal of uncertainty exists regarding the allowable deflection before separation near the hinge line.

The present study examines a turbulent boundary layer past convex corners at high subsonic Mach numbers (Fig. 1). This corresponds to a simplified configuration that models the deflection of a control surface. The investigation involves the high subsonic flow pasts a convex corner, which gives rise to attached or separated flow. Oil-flow visualization and measurements of surface static pressure were conducted to study the interaction region and separation criteria for the transonic convex-corner flows. In addition, the shock-induced separated boundary layer is usually associated with the low-frequency, large-scale oscillation of a shock wave.[7] Measurements of surface pressure fluctuations were conducted to study the unsteadiness of the flows. This is essentially required for the flow-induced vibration of aerodynamic devices. Before discussing the results of present study, brief details of the experiment are outlined next.

Experiment

Transonic Wind Tunnel

The Aerospace Science and Technology Research Center/National Cheng Kung University (ASTRC/NCKU) transonic wind tunnel is a blowdown type.[8] The operating Mach number ranges from 0.2 to 1.4, and the simulated Reynolds number is up to 2×10^7/m. Major components of the facility include compressors, air dryers, a cooling water system, storage tanks, and the tunnel. The dew point of high-pressure air through the dryers is maintained at -40°C under normal operation conditions. Air storage volume for the three storage tanks is up to 180 m^3 at 5.15 MPa. The test section is 600 mm square and 1500 mm long. In the present study, the test section was assembled with solid sidewalls and perforated top/bottom walls. The freestream Mach numbers M_∞ are 0.64 and 0.83 ± 0.01. The stagnation pressure p_0 and temperature T_0 are 172 ± 0.5 kPa and room temperature, respectively, for all of the tests.

For the data acquisition system, the Neff Instruments System 620 and the LeCroy waveform recorders were used. The test conditions were recorded by the Neff system, whereas the LeCroy 6810 waveform recorders were used for the surface pressure measurements. A host computer with CATALYST software controls the setup of LeCroy waveform recorders through a LeCroy 8901A interface. All input channels were triggered simultaneously by using an input channel as the trigger source.

Received 22 June 2001; revision received 28 May 2002; accepted for publication 29 May 2002.

*Associate Research Fellow, Aerospace Science and Technology Research Center, 2500 Section 1, Chung-Jang South Road, Kueijen. Senior Member AIAA.

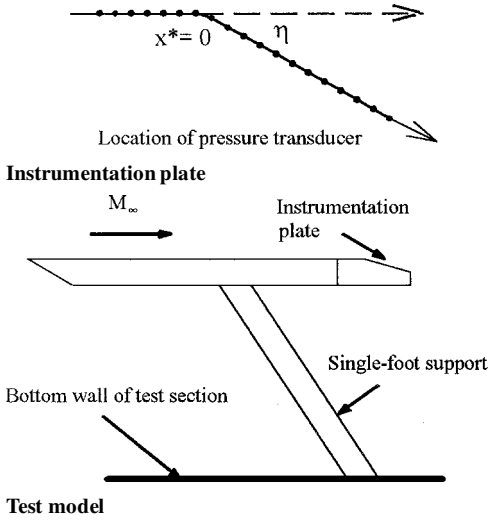

Fig. 1 Test configuration.

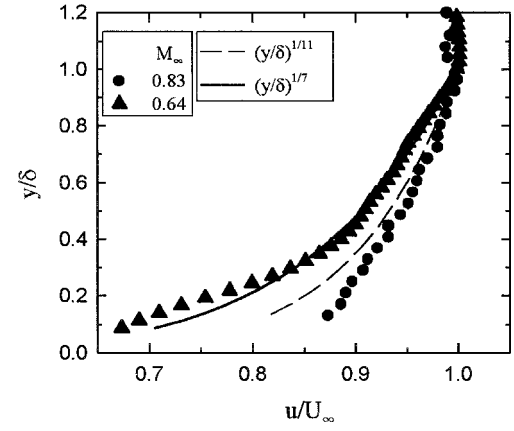

Fig. 2 Normalized incoming boundary-layer profiles.

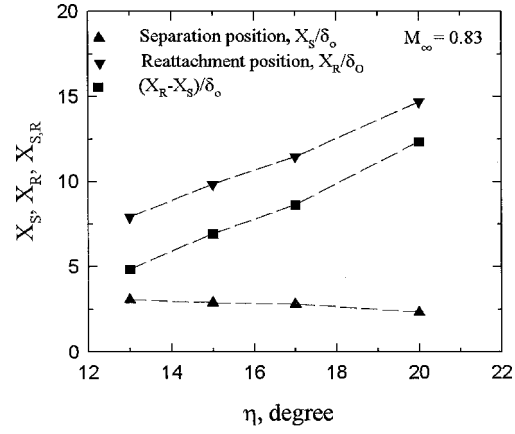

Fig. 3 Separation length.

Test Model

The test model consists of a flat plate and an interchangeable instrumentation plate. The test model is 150 mm wide and 600 mm long and was supported by a single sting mounted on the bottom wall of the test section. The corner, with 5-, 10-, 13-, 15-, 17-, and 20-deg convex-cornerangle η, is located at 500 mm from the leading edge of the flat plate. One row of 19 pressure taps for the installation of flush-mounted pressure transducers, 6 mm apart and 2.5 mm in diameter, was drilled perpendicularly to the test surface along the centerline of each instrumentation plate. The side fences at both sides of the instrumentation plate were used to prevent crossflow.

Experimental Techniques

For the surface pressure measurements, the Kulite pressure transducers (Model XCS-093-25A, B screen) powered by a Topward Electronic System Model 6102 power supply at 15.0 V were used. The outside diameter is 2.36 mm, and the sensing element is 0.97 mm in diameter. The natural frequency is 200 kHz as quoted by the manufacturer. All of the pressure transducers were flush mounted and potted using silicone rubber sealant. Flushness of the pressure transducers was checked by a machinist's block to minimize the interference with the flow. External amplifiers (Ecreon Model E713) were used to improve the signal-to-noise ratio. With a gain of 20, the rolloff frequency is about 140 kHz. In addition, note that there is high-frequency damping due to the transducer's size. According to the Corcos's criterion,[9] the maximum measurable frequency $f_{\max}$ of a pressure transducer under a given flow condition is equal to $U_c/2\pi r$, where r is the radius of pressure transducer and U_c is the convection velocity. Under the assumption that $U_c = 0.8U_\infty$, the $f_{\max}$ is about 63 kHz in the present study. However, Gramann and Dolling[10] indicated that the perforated screen of the Kulite pressure transducer might limit the frequency response only up to 50 kHz. Furthermore, the typical sampling period in the present study is 5 μs (200 kHz). Each data record possesses 131,072 data points for the statistical analysis. The data were divided into 32 blocks. The mean and fluctuating values of each block (4096 data points) were calculated. Variations of the blocks were estimated to be 0.43 and 0.13% for the mean surface pressure coefficient C_p and the fluctuating pressure coefficient C_{σ_p}, respectively, which are considered as the uncertainty of experimental data.

The oil-flow visualization technique is used to check the two dimensionality of the flow and to visualize the surface flow pattern. A thin film of the mixture (titanium dioxide, oil, oleic acid, and kerosene) is applied on the surface of instrumentation plate. The region of separation and reattachment was visualized and compared with the surface pressure measurements. In addition, the normalized velocity profiles for the undisturbed boundary layer at 25 mm upstream of the convex corner appear to be full ($n \approx 7$–11 for the velocity power law) (Fig. 2). This indicates turbulent flow at the measurement locations. The boundary-layer thickness is estimated to be 7.3 and 7.1 $\pm$ 0.2 mm, and the Reynolds number Re_{δ_0} is 14.9 and 16.8 $\times$ 10^4 for Mach 0.64 and 0.83, respectively.

Results and Discussions

Oil-Flow Pattern

Because of the limited size of the test model, it is necessary to consider whether the flow near the centerline downstream of the corner surface is representative of the flow over a similar corner of infinite span. The typical oil-flow pattern for an attached flow, for example, $M_\infty = 0.83$ and $\eta = 5$ deg, shows that the streamlines over the whole span are straight and parallel to the incoming flow direction. At $M_\infty = 0.83$ and $\eta = 10$ deg, the nearly straight streamlines are also observed. However, accumulation of titanium dioxide is observed at $x \approx 17 \sim 31$ mm. This is considered to be due to the stronger adverse pressure gradient or the initial separation of the boundary layer. When the convex angle further increases ($M_\infty = 0.83$ and $\eta = 13$ deg), accumulation of titanium dioxide is more evident followed by the deflection of streamlines. The beginning of accumulation is taken as the separation position X_S. At a position farther downstream, the end of deflection is taken as the reattachment position X_R. The similar feature is also obtained for the other cases at higher convex-corner angle with a more extensively separated boundary layer. Observation of the oil-flow patterns for all of the cases of separated flow is summarized in Fig. 3. Note that the separation bubble grows in both upstream and downstream directions with increasing η, in which the separation position moves slightly upstream and the reattachment position moves downstream. The separation length ($X_R - X_S$), which is defined as the distance between the separation and reattachment positions, appears to increase linearly with the convex-cornerangle for the present test cases. This shows results similar to those in the study by Liu and Squire[3] on the

circular-arc models, in which the separation length increases with surface curvature at a given peak Mach number upstream of shock position.

Mean Surface Pressure Distributions

The distributions of mean surface pressure coefficient C_p along the centerline of the instrumentation plates are plotted in Figs. 4 and 5, where the sonic condition is also shown for reference. The origin of the x coordinate is set at the corner. The distributions appear similar in shape for all of the test cases. The flows accelerate upstream of the convex corner, which is due to the effect of displacement thickness on the effective local wall surface. The minima are observed immediately downstream of the corner, followed by the recompressions. For $M_\infty = 0.64$ at $\eta \leq 15$ deg, and $M_\infty = 0.83$ at $\eta = 5$ deg ($M_\infty^2 \eta \leq 6.14$) (Ref. 11), the flowfield appears to be a pure expansion and recompression type (or a subsonic expansion flow). Stronger upstream expansion and steeper downstream recompression are associated with the increasing η. It is also observed that the level of C_p tends to a nearly constant value at locations farther downstream and decreases with larger η. For $M_\infty = 0.64$ at $\eta \geq 17$ deg, and $M_\infty = 0.83$ at $\eta \geq 10$ deg ($8.19 \geq M_\infty^2 \eta > 6.14$), there is stronger upstream expansion, and the flow expands to supersonic immediately downstream of the corner. The flow switches from a subsonic to a transonic type. The transonic expansion flow results in a milder initial recompression downstream of the corner, and the supersonic region may extend throughout the measurement location at higher $M_\infty^2 \eta$. This implies that the shock wave pattern may change from a single normal shock wave to a lambda shock wave or a possible Mach reflection. For $M_\infty = 0.83$ at $\eta \geq 13$ deg ($M_\infty^2 \eta \geq 8.95$), it is found that there is a distinctive kink at $x^* \approx 3$ in the C_p distribution. This indicates that the shock wave separates the boundary layer, which agrees with the oil-flow visualization. A slower recovery process is associated with a more extensively separated boundary layer, which also induces a larger interaction region.

Fluctuating Pressure Distributions

Other than the mean pressure data, the measurements of surface pressure fluctuation were also analyzed. The distributions of normalized surface pressure fluctuation are shown in Figs. 6 and 7. The surface pressure fluctuation coefficient C_{σ_p} represents the increase of surface pressure fluctuations with respect to the freestream condition. In Fig. 6 ($M_\infty = 0.64$), it can be seen that C_{σ_p} increases upstream of the convex corner and reaches the maximum at a location immediately downstream. The rise of C_{σ_p} corresponds to the initial pressure rise of mean surface pressure. For the subsonic expansion flows ($\eta \leq 15$ deg), the peaks $C_{\sigma_p,\max}$ are considerably lower than those of the transonic expansion flows ($\eta \geq 17$ deg) and the level of C_{σ_p} returns to the value of the upstream undisturbed boundary layer more quickly. At $M_\infty = 0.83$, the C_{σ_p} distribution at $\eta = 5$ deg shows a similar trend as that of a subsonic expansion flow at $M_\infty = 0.64$. However, the C_{σ_p} decreases initially near the corner at larger η (transonic expansion flow). This corresponds to the strong upstream expansion. For the cases of separated boundary layer ($\eta \geq 13$ deg), the C_{σ_p} increases rapidly downstream of the corner and reaches the maximum ahead of the separation point ($X_S^* \approx 2.5$). The magnitude of $C_{\sigma_p,\max}$ reaches about 9% of the dynamic pressure q_∞. This characteristic is similar to the case of a two-dimensional ramp flow,[12] and the maximum surface pressure fluctuations are essentially related to the oscillation of the shock wave. Further downstream, the plateau level of pressure fluctuations increases slightly with the increasing η. The surface pressure fluctuations normalized by the local wall

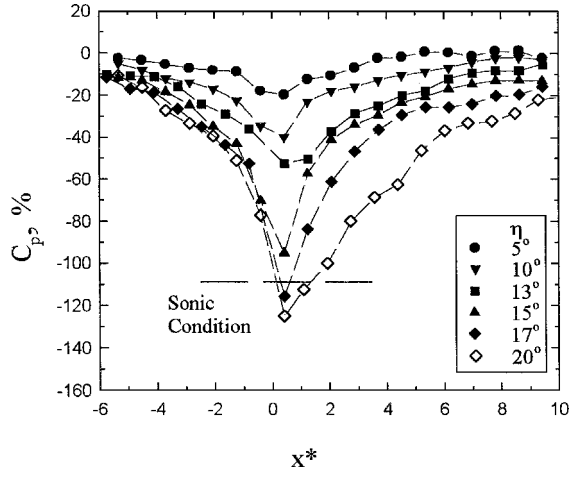

Fig. 4 Mean surface pressure distributions, $M_\infty = 0.64$.

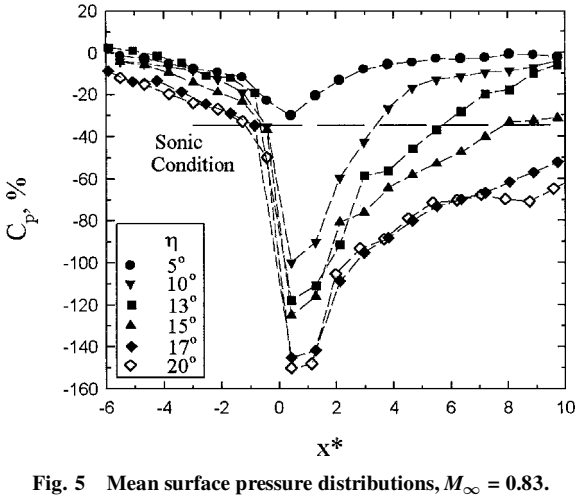

Fig. 5 Mean surface pressure distributions, $M_\infty = 0.83$.

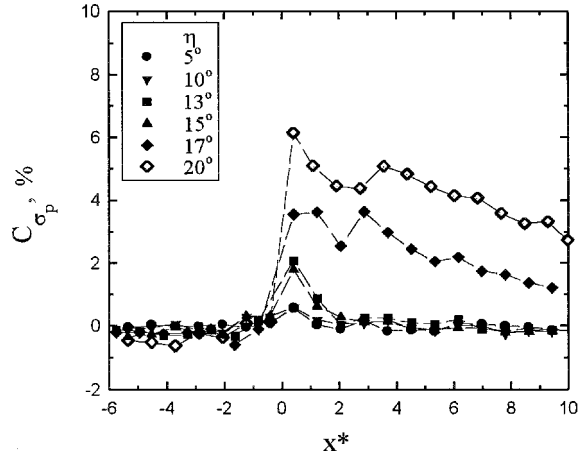

Fig. 6 Surface pressure fluctuation distributions, $M_\infty = 0.64$.

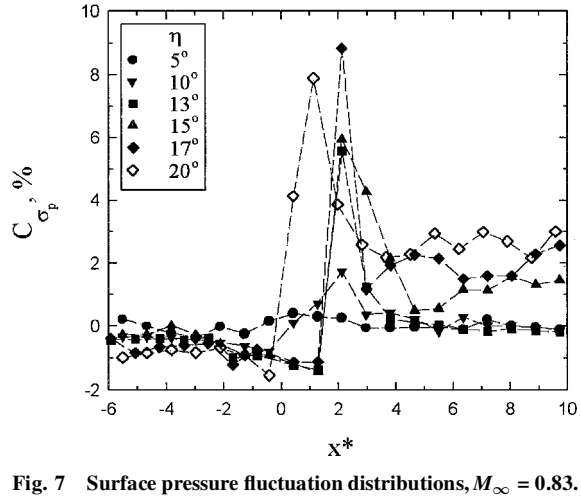

Fig. 7 Surface pressure fluctuation distributions, $M_\infty = 0.83$.

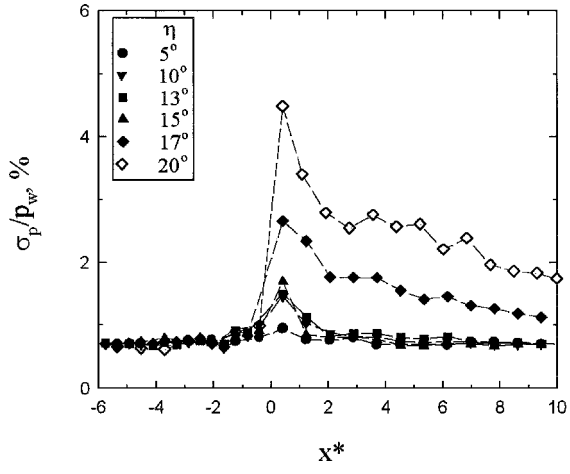

Fig. 8 Normalized surface pressure fluctuations using p_w, $M_\infty = 0.64$.

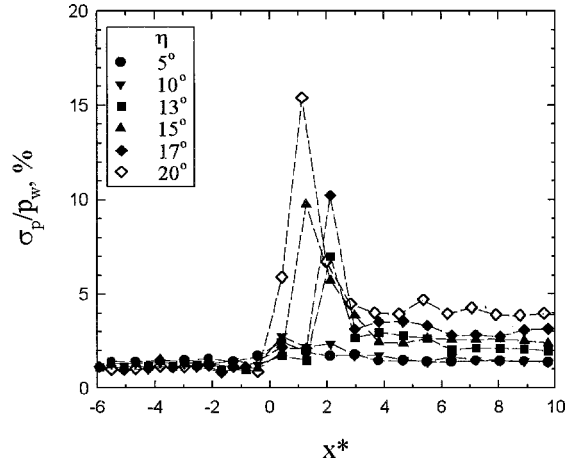

Fig. 9 Normalized surface pressure fluctuations using p_w, $M_\infty = 0.83$.

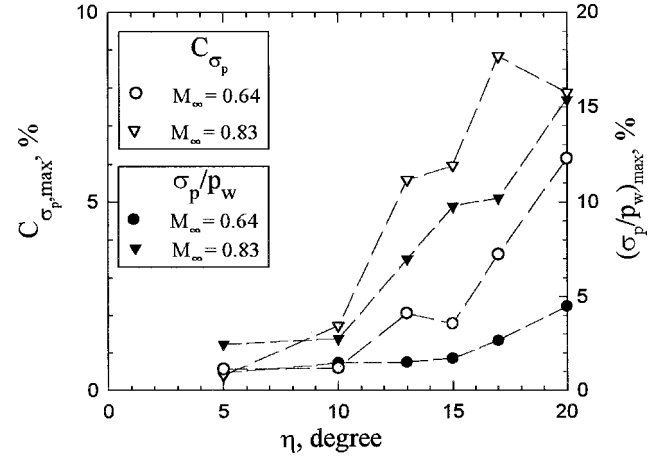

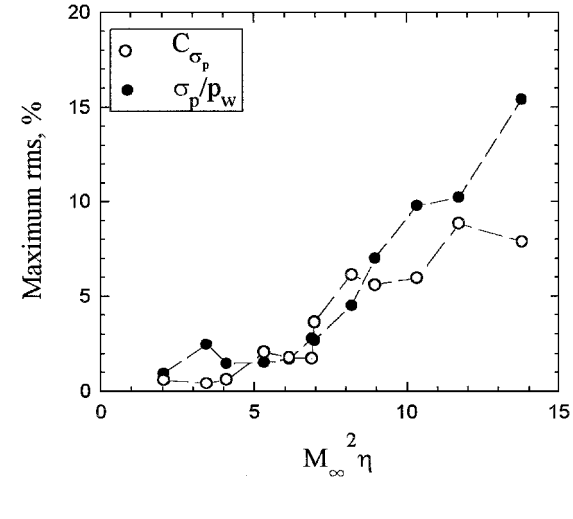

Fig. 10 Maximum normalized surface pressure fluctuations.

pressure p_w are shown in Figs. 8 and 9. The σ_p/p_w corresponds to the local variation of surface pressure fluctuations. It can be seen that the σ_p/p_w distributions show the similar trend as those of C_{σ_p}. The visible peaks, which are up to 15% of local wall pressure, are observed downstream of the corner, and the magnitude increases with M_∞ and η. Farther downstream, the amplitude of σ_p/p_w appears to be approaching a nearly constant level. For the subsonic expansion flows, it is estimated that the new equilibrium level of σ_p/p_w would be reached at about $3–4\delta_0$. This agrees with the measurements of mean surface pressure distributions. However, the σ_p/p_w curves for $M_\infty = 0.64$ at $\eta = 17$ and 20 deg (transonic expansion flows) show a slower recovery process. For the cases of a separated boundary layer ($M_\infty = 0.83$ at $\eta \geq 13$ deg), the σ_p/p_w decreases toward the separation location after the peak value. The new equilibrium levels of σ_p/p_w increase with η (or shock strength).

The $C_{\sigma_p,\max}$ and $(\sigma_p/p_w)_{\max}$, Fig. 10a, can be used for the indication of flow unsteadiness. The present study indicates that the type of expansion flow and characteristics of the boundary layer have a strong effect on the amplitude of peak surface pressure fluctuations. In general, the $C_{\sigma_p,\max}$ and $(\sigma_p/p_w)_{\max}$ increase only slightly with increasing η for the subsonic expansion flows. For the transonic expansion flows, the levels of $C_{\sigma_p,\max}$ and $(\sigma_p/p_w)_{\max}$ are considerably higher than those of the subsonic expansion flows. The study of Chung[11] indicated that transition of the subsonic and transonic expansion flows could be scaled with $M_\infty^2\eta$. The data of $C_{\sigma_p,\max}$ and $(\sigma_p/p_w)_{\max}$ are replotted as shown in Fig. 10b. It can be seen that the correlations of $C_{\sigma_p,\max}$ and $(\sigma_p/p_w)_{\max}$ with $M_\infty^2\eta$ agree reasonably well. A gradual increase can be seen for $M_\infty^2\eta \leq 6.14$. For the transonic expansion flows, the $C_{\sigma_p,\max}$ and $(\sigma_p/p_w)_{\max}$ increase more rapidly with $M_\infty^2\eta$. This implies that the unsteadiness of the transonic convex-corner flows is associated with the convex-corner angle and the second-order effect of freestream Mach number.

Conclusions

Oil-flow visualization is used to visualize the surface flow pattern of the subsonic and transonic expansion flows. The boundary layer is separated at $M_\infty^2\eta \geq 8.95$. Separation position moves slightly upstream and reattachment position moves downstream with the increasing convex-corner angle, in which the separation length increases with increasing convex-corner angle. Measurements of the mean and fluctuating surface pressures have also been conducted along the centerline of the instrumentation plates. For the subsonic expansion flows, the presence of the convex corner in a turbulent boundary layer results in strong upstream expansion and downstream recompression. The interaction region depends on the freestream Mach number and the convex-corner angle. The transonic expansion flows result in milder initial recompression downstream of the corner, and the supersonic region may extend throughout the measurement location at higher $M_\infty^2\eta$. The measurements of surface pressure fluctuations indicate the intermittent nature of the pressure signals for the transonic expansion flows. The unsteadiness of the flows is related to the type of expansion flow and the shock wave oscillation, and the amplitude of peak pressure fluctuations could be scaled with $M_\infty^2\eta$. For the cases of separated boundary layer, the peak surface pressure fluctuations are observed upstream of the separation point and increase significantly.

Acknowledgments

The research is support by National Science Council (NSC 89-2612-E-006-019). The support is gratefully acknowledged. The

author also acknowledges the technical support of the Aerospace Science and Technology Research Center/National Cheng Kung University technical staff during the experiments.

References

[1]Inger, G. R., "Transonic Shock/Turbulent Boundary-Layer Interaction and Incipient Separation on Curved Surfaces," AIAA Paper 81-1244, June 1981.

[2]Delery, J. M., "Experimental Investigation of Turbulent Properties in Transonic Shock/Boundary-Layer Interactions," *AIAA Journal*, Vol. 21, No. 11, 1983, pp. 1628–1634.

[3]Liu, X., and Squire, L. C., "An Investigation of Shock/Boundary Layer Interactions on Curved Surfaces at Transonic Speeds," *Journal of Fluid Mechanics*, Vol. 187, 1988, pp. 467–486.

[4]Bolonki, A., and Gilyard, G. B., "Estimated Benefits of Variable-Geometry Wing Camber Control for Transport Aircraft," NASA TM-1999-206586, Oct. 1999.

[5]Szodruch, J., and Hilbig, R., "Variable Wing Camber for Transport Aircraft," *Progress in Aerospace Sciences*, Vol. 25, No. 3, 1988, pp. 297–328.

[6]Greff, E., "Aerodynamic Design and Integration of a Variable Camber Wing for a New Generation Long/Medium Range Aircraft," International Council of the Aeronautical Sciences, Paper ICAS 88-2.2.3, Aug. 1988.

[7]Muck, K., Andreopoulos, J., and Dussauge, J., "Unsteady Nature of Shock Wave/Turbulent Boundary-Layer Interaction," *AIAA Journal*, Vol. 26, No. 2, 1988, pp. 179–187.

[8]Chung, K., "Development and Calibration of ASTRC/NCKU 600 mm × 600 mm Transonic Wind Tunnel," National Science Council Grant Rept. NSC 83-2212-E-006-141T, Aug. 1994.

[9]Corcos, G. M., "Resolution of Pressure in Turbulence," *Journal of the Acoustical Society of America*, Vol. 35, No. 2, 1963, pp. 192–199.

[10]Gramann, R. A., and Dolling. D. S., "Detection of Turbulent Boundary-Layer Separation Using Fluctuating Wall Pressure Signals," *AIAA Journal*, Vol. 28, No. 6, 1990, pp. 1052–1056.

[11]Chung, K., "Transition of Subsonic and Transonic Expansion-Corner Flows," *Journal of Aircraft*, Vol. 37, No. 6, 2000, pp. 1079–1082.

[12]Dolling, D. S., and Or, C. T., "Unsteadiness of the Shock Wave Structure in Attached and Separated Compression Ramp Flows," *Experiments in Fluids*, Vol. 3, No. 1, 1985, pp. 24–32.